Real Time Determination of the Electronic Structure of Unstable Reaction Intermediates during Au2O3 Reduction

ARTICLE *in* JOURNAL OF PHYSICAL CHEMISTRY LETTERS · JANUARY 2014

Impact Factor: 7.46 · DOI: 10.1021/jz402309s

9 AUTHORS, INCLUDING:

Jacinto Sa
Paul Scherrer Institut
43 PUBLICATIONS **405** CITATIONS

J-Cl Dousse
Université de Fribourg
165 PUBLICATIONS **1,616** CITATIONS

Hongqing Shi
27 PUBLICATIONS **323** CITATIONS

Catherine Stampfl
University of Sydney
216 PUBLICATIONS **6,498** CITATIONS

THE JOURNAL OF PHYSICAL CHEMISTRY Letters

Letter

pubs.acs.org/JPCL

Real Time Determination of the Electronic Structure of Unstable Reaction Intermediates during Au_2O_3 Reduction

Jakub Szlachetko,*[†,‡,∇] Jacinto Sá,[†,§,∇] Maarten Nachtegaal,[†] Urs Hartfelder,[†,⊥] Jean-Claude Dousse,[#] Joanna Hoszowska,[#] Daniel Luis Abreu Fernandes,[∥] Hongqing Shi,[¶] and Catherine Stampfl*[¶]

[†]Paul Scherrer Institut, Villigen, Switzerland

[‡]Institute of Physics, Jan Kochanowski University, Kielce, Poland

[§]LSU Group, École Polytechnique Fédérale de Lausanne (EPFL), Lausanne, Switzerland

[⊥]Department for Chemical and Bioengineering, ETH Zurich, Zurich, Switzerland

[#]Department of Physics, University of Fribourg, Fribourg, Switzerland

[∥]Department of Chemistry, University of Aveiro, Aveiro, Portugal

[¶]School of Physics, The University of Sydney, Sydney, Australia

Supporting Information

ABSTRACT: Chemical reactions are always associated with electronic structure changes of the involved chemical species. Determining the electronic configuration of an atom allows probing its chemical state and gives understanding of the reaction pathways. However, often the reactions are too complex and too fast to be measured at in situ conditions due to slow and/or insensitive experimental techniques. A short-lived Au_2O compound has been detected for the first time under in situ conditions during the temperature-programmed reduction of Au_2O_3. A time-resolved resonant inelastic X-ray scattering experiment (RIXS) allowed the determination of changes in the Au electronic structure, enabling a better understanding of the reaction mechanism of Au(III) reduction. On the basis of time-resolved RIXS data analysis combined with genetic algorithm methodology, we determined the electronic structure of the metastable Au_2O intermediate species. The data analysis showed a notably larger value for the lattice constant of the intermediate Au as compared to the theoretical predictions. With support of DFT calculations, we found that such a structure may indeed be formed and that the expanded lattice constant is due to the termination of Au_2O on the Au_2O_3 structure.

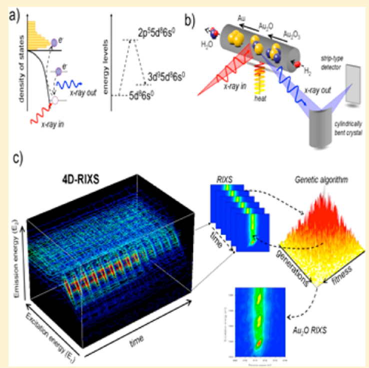

SECTION: Spectroscopy, Photochemistry, and Excited States

Chemical reactions are driven by the electronic structure of the valence shell of the catalytic active metal. The availability of valence orbitals to form chemical bonds, and thus take part in the chemical reaction, depends on their electron occupancy and energy.[1,2] Therefore, the characterization of the electronic structure of catalysts before, during, and after a reaction is vital for the fundamental understanding of materials performance and stability.

Resonant inelastic X-ray scattering (RIXS) spectroscopy offers great potential to study the electronic structure of the catalytic site. RIXS is a photon-in, photon-out scattering technique where the incoming photon excites the atom to an intermediate state, which decays to its final state by the emission of a photon. RIXS combines X-ray absorption, which reflects the unoccupied density of states (DOS) and X-ray emission processes, which characterizes the occupied DOS and thus allows for a detailed investigation of the local electronic structure of the metal of interest. Furthermore, thanks to the penetrating properties of hard X-rays, RIXS can be performed in situ, thus providing information about occupied and unoccupied electronic states of catalysts under working conditions.[3−7] Moreover, the RIXS has been recognized as a most powerful technique, as compared to commonly applied X-ray absorption spectroscopy (XAS) techniques, to study the electronic structure of matter.[8]

To obtain meaningful information, RIXS spectroscopy requires high-energy resolution for both the incoming and outgoing X-rays. To this point, RIXS spectroscopy has been restricted to the investigation of steady-state systems because of the relatively long acquisition times imposed by the necessity of scanning the incoming and outgoing X-ray energies with high energy resolution during the experiment.[9−11]

Herein, we report on the changes occurring in the electronic structure of Au during the temperature-programmed reduction of Au_2O_3. The electronic structure was monitored by time-resolved RIXS spectroscopy using a von Hamos type crystal

Received: October 25, 2013
Accepted: December 6, 2013
Published: December 6, 2013

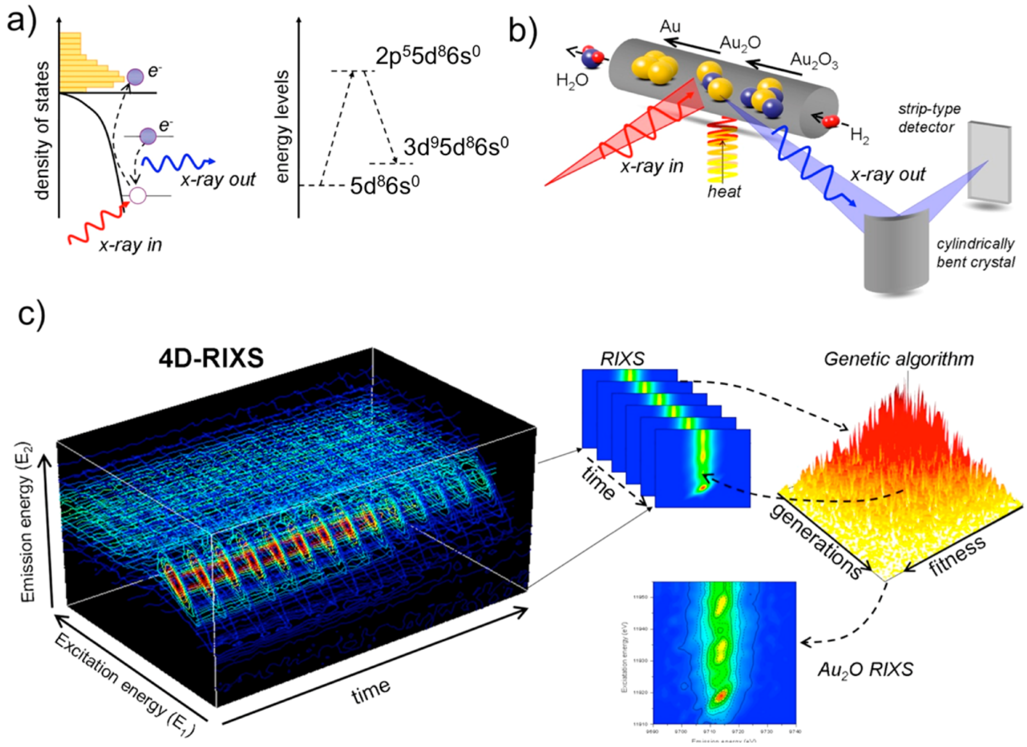

Figure 1. (a) Schematic representation of the RIXS process in a Au atom. The incoming X-ray excites a core electron above the Fermi level (intermediate state). The core hole is then filled by an electron from a higher atomic level with the simultaneous emission of an X-ray (final state). (b) Experimental setup for time-resolved RIXS. The Au_2O_3 powder is enclosed in a reactor cell and heated up in a reducing H_2 environment. RIXS is recorded by continuous scanning of the incoming X-ray energy while detecting the emitted X-ray energies in a dispersive fashion. (c) Time evolution of the RIXS spectra during the experiment (time-resolved RIXS) and schematics of the data analysis procedure employing genetic algorithm computations for the extraction of the intermediate Au_2O electronic structure from the time-resolved RIXS.

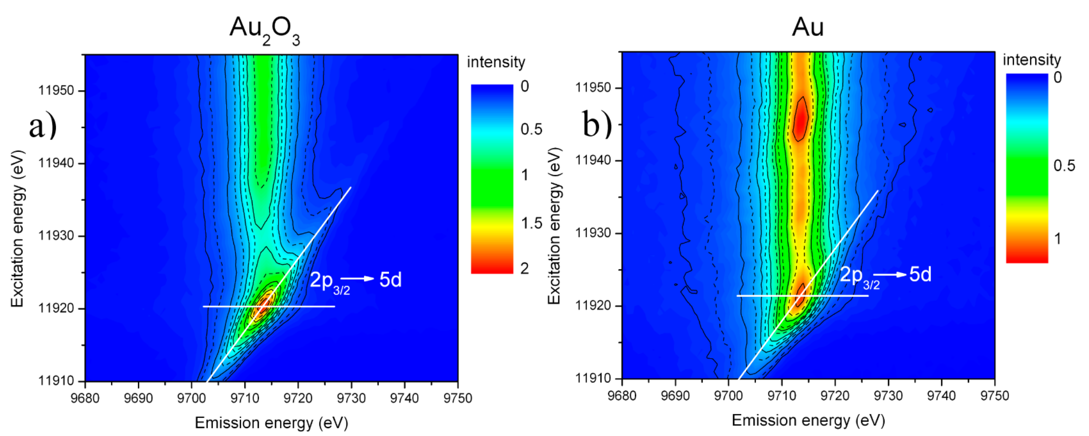

Figure 2. (a) RIXS plane of Au_2O_3 recorded at low temperatures. (b) RIXS plane of Au(0) after Au_2O_3 reduction. A complete change in the electronic structure and 5d population density together with an energy shift of the $2p_{3/2} \rightarrow 5d$ resonance is observed. The solid white lines mark the $2p_{3/2} \rightarrow 5d$ resonance and its maximum.

spectrometer.[12,13] Because of the dispersive-type detection of the emitted X-rays, only the energy of the incoming X-rays is scanned; thus, the RIXS planes can be recorded at sub-minute time resolution. The recorded electronic structure changes reveal the existence of a short-lived metastable Au(I) oxide in the temperature-programmed reduction of Au_2O_3, whose electronic and geometric properties could be retrieved from the time-resolved RIXS data set with the help of a genetic algorithm.

Figure 1a shows the schematics of the RIXS process around the L_3 absorption edge of Au(III). By tuning the incoming X-ray energy around the L_3 edge ($2p_{3/2}$ electrons), the density of the unoccupied 5d states can be probed with high sensitivity thanks to the strong $2p_{3/2} \rightarrow 5d$ dipolar excitation. Within 0.11 fs,[14] the $2p_{3/2}$ core hole decays then via the $3d_{5/2} \rightarrow 2p_{3/2}$ electronic transition; this is accompanied by the emission of an X-ray photon. Therefore, by monitoring the incoming and outgoing X-ray energies/intensities, detailed information about the electronic structure of Au[10] can be retrieved. In the present experiment, Au_2O_3 powder was loaded into a quartz capillary reactor connected to a H_2 inlet. The sample was heated from 20 up to 300 °C with a ramp of 5 °C per minute. The electronic

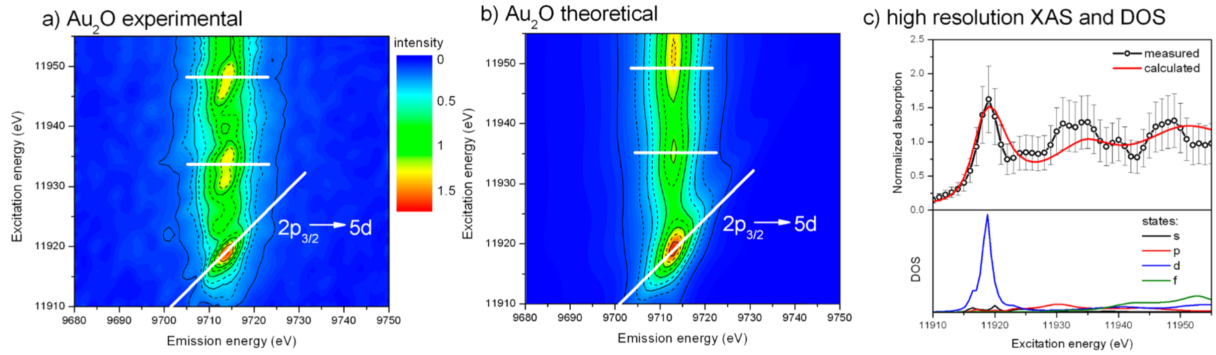

Figure 3. (a) Extracted RIXS plane of Au_2O from the time-resolved RIXS data set compared to theoretical calculations (b). (c) Comparison between the extracted high energy resolution X-ray absorption spectrum and the corresponding theoretical predictions. The contribution of the DOS of the different orbitals to the X-ray absorption spectrum is plotted in the bottom panel.

structure of Au was then continuously monitored by means of time-resolved RIXS spectroscopy with a time resolution of 55 s (Figure 1b). In total, 70 RIXS planes were recorded that contain information about the Au electronic structure changes during the temperature rise. The data are illustratively plotted in the form of a 4D representation in Figure 1c.

The temperature-programmed reduction of the Au_2O_3 compound leads to its reduction to metallic Au at temperatures of around 130–200 °C.[15,16] This was confirmed by the RIXS experiment. The representative RIXS planes of the starting Au(III) and end Au(0) states are plotted in Figure 2. The Au_2O_3 RIXS plane is characterized by a strong $3p_{3/2} \rightarrow 5d$ resonance at an excitation energy of around 11920 eV that is present due to the partially unfilled $5d^8$ orbital. This resonance is much weaker in the case of Au(0), where the 5d orbital is almost completely filled. The $3p_{3/2} \rightarrow 5d$ excitation in Au(0) can be observed only because of strong hybridization of 6s–5d orbitals.[17] Also, a small energy shift of ~2 eV in the $3p_{3/2} \rightarrow 5d$ resonance maximum of Au(III) and Au(0) phases was detected, in agreement with previous X-ray absorption data.[18] In summary, the RIXS planes show distinct features in the electronic structures that are representative of each of the two end states.

To recover the concentration changes of Au(III) and Au(0) during the temperature-programmed reduction experiment, the representative RIXS planes of Figure 2 were used as references to fit the 70 time-resolved RIXS spectra. The least-squares fitting procedure and analysis of fit residuals revealed that at intermediate temperatures of 140–200 °C, the experimental data could not be reproduced using only those two references. This result suggested the existence of a third Au phase (see the Supporting Information (SI) for details). In order to extract the electronic structure of this third component from the experimental data, we applied the genetic algorithm procedure[19,20] (see the SI for details). The outcome of the computation is presented in Figure 3. As shown, the RIXS plane of the intermediate Au consists of a 5d resonance with a maximum located at an excitation energy of 11919.5 eV. This resonance is weaker in intensity than the one observed in the case of Au_2O_3 but stronger than that in the case of Au(0). Furthermore, weak structures were detected at higher excitation energies, at around 11934 and 11948 eV, respectively. The detection of a third component in the time-resolved RIXS data suggests that the Au_2O_3 reduction occurs in two steps, possibly with the formation of Au(I) according to the following reaction path:

$$Au_2O_3 + 2H_2 \rightarrow Au_2O + 2H_2O$$

$$Au_2O + H_2 \rightarrow Au^0 + H_2O$$

Despite being a credible and possible reduction mechanism, evidence for Au_2O formation is scarce. The main reason is that Au(I) oxide is an endothermic system and metastable with respect to O_2 and metallic Au.[21] As predicted by theoretical calculations, the bulk Au_2O phase forms into the cuprite structure with a fcc lattice.[18] We used this theoretical structure estimation to calculate the electronic DOS of Au using the FEFF9.0 code[22,23] and the Kramers–Heisenberg formulas for the RIXS process.[24] The calculated RIXS plane is presented in Figure 3b. As shown, good agreement was achieved with the experimental data because all three RIXS features could be well-reproduced. The agreement is particularly good around the edge. The discrepancy in the post-edge region relates to the fact that the features in this region are naturally broad due to multiple scattering processes; however, the features are detectable within the measurement error. In Figure 3c, we plot the high energy resolution X-ray absorption spectrum extracted from the peak intensity variation of the $L_{\alpha 1}$ transition. The spectrum is compared to the theoretical one, together with the DOS of Au in the Au_2O structure. Similar to Au(III) and Au(0), the Au(I) oxide white line is composed of unoccupied d orbitals, while the s, p, and f states do not contribute significantly to the spectrum. The two structures at higher excitation energies relate to the multielectron scattering effects, the contribution from other orbitals being negligible.[14]

We should note here that in order to match the theoretical calculations with the experimental RIXS data, the lattice constant of the Au(I) oxide in the fcc form had to be expanded from 4.8 to 5.3 Å. For the temperature at which the Au(I) oxide was detected (140–200 °C), this relatively big mismatch cannot be explained by thermal expansion.[25−27] The reduction of the Au_2O_3 particle follows a shell-to-core mechanism, where first the outside of the particle is reduced. The process then continues constantly from the outer shell to the inside of the particle. In this case, the Au(I) oxide may be formed in the sample as a thin layer located between the Au_2O_3 and Au(0) structures. For this reason, we investigated how the Au_2O phase would terminate on the Au_2O_3 structure.

In order to validate the Au_2O termination hypothesis, we performed surface formation energy calculations using the DFT total energy Vienna ab initio simulation package (VASP).[28−31] To investigate the relative stability of a thin layer of $Au_2O(001)$ on $Au_2O_3(001)$ (see Figure 4a and b) as compared to the

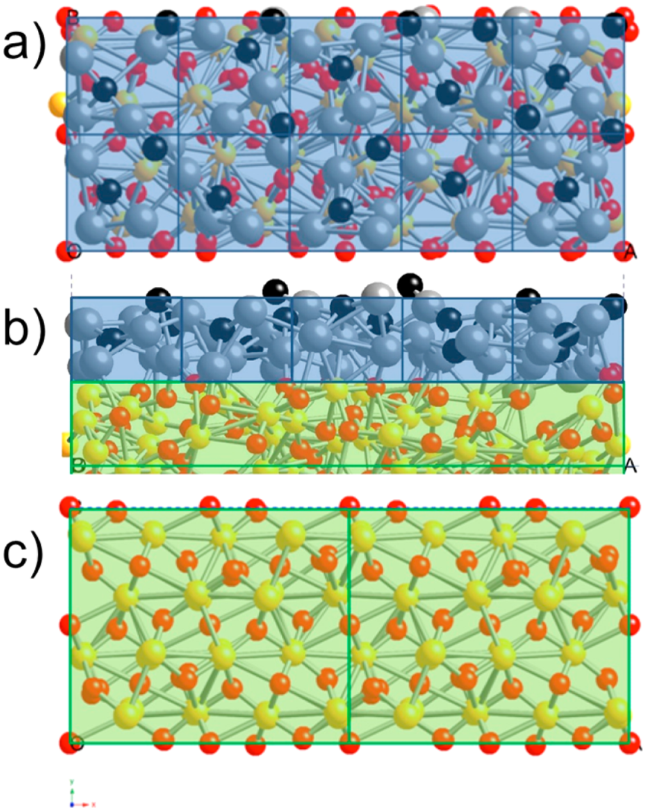

Figure 4. (a) Top view of the atomic structure of Au_2O on Au_2O_3 and (b) the side view. The layer of Au_2O is shaded gray. The smaller and larger spheres indicate oxygen and gold atoms, respectively. (c) The top view of the two surface unit cells of $Au_2O_3(001)$.

unreconstructed $Au_2O_3(001)$ surface (Figure 4c), we used the approach of ab initio atomistic thermodynamics.[32] We employed the projector augmented wave method[33,34] (PAW) and the generalized gradient approximation (GGA) for the exchange−correlation functional[35] (for details, see the SI). The simulations showed that at zero temperature and O-rich conditions (delta O-chem pot = 0), the two-layer Au_2O_3 structure has the lowest formation energy, but for increasing temperature, the one-layer Au_2O on Au_2O_3 becomes lower in energy (delta O-chem pot ≅ −0.1 eV). This is consistent with the fact that the time-resolved RIXS experiment detects the presence of Au_2O. What should be also noticed is that the lattice constant in the *b* direction of Au_2O_3 is around 10.68 Å. This is approximately twice as much as the value of 5.3 Å found for the Au_2O lattice constant (10.68 Å/2 = 5.34 Å). Further, the lattice constant of Au_2O_3 in the *a* direction is around 13.06 Å, and this value multiplied by 2 (26.12 Å) is about five times bigger than 5.3 Å (26.12 Å/5 = 5.23 Å). In summary, this means that the surface of 10 unit cells of $Au_2O(001)$ fits the surface of 2 (along the *a* axis) × 1 (along the *b* axis) $Au_2O_3(001)$ unit cells. The latter is in agreement with the experimental results and confirms the detection of the Au_2O phase with an expanded lattice parameter as a termination structure of Au_2O_3.

Using the three RIXS references of Au phases, we employed least-squares fitting to the time-resolved data in order to follow the concentration of Au species as a function of temperature. The outcome of the fitting is plotted in Figure 5. The Au_2O_3 reduction starts at temperatures of around 100 °C with a smooth decrease in concentration of about 10−20% up to 180

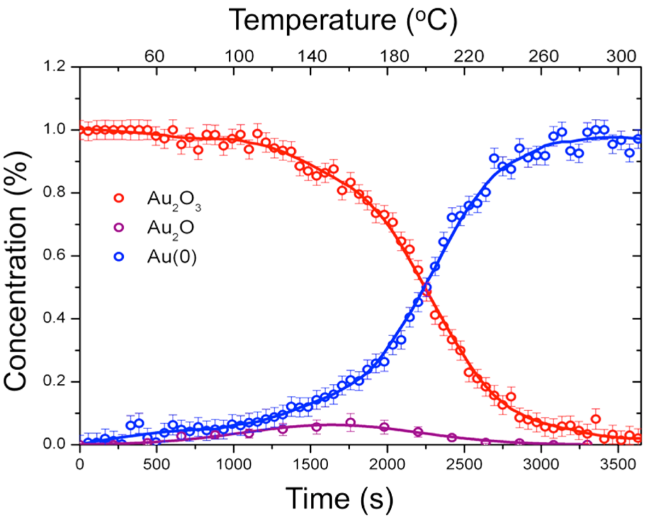

Figure 5. Concentration changes of Au_2O_3, Au_2O, and Au(0) during the temperature-programmed reduction of Au_2O_3. The data are plotted versus time (bottom scale) and temperature (top scale).

°C. A quick decrease is detected at temperatures of 180−220 °C with simultaneous increase of the Au(0) concentration. At a temperature of 200 °C, a 50/50 ratio between Au_2O_3 and Au is detected. The intermediate Au_2O species are detected at temperatures of 100−200 °C and at a maximum level of concentration of about 7−8%. This low level of detected Au_2O, as compared to the other two species, is synonymous with the fact that, once formed, the Au_2O is quickly reduced to Au(0), that is, a short-lived intermediate. The observation confirms that Au_2O is involved in the reduction of Au_2O_3 to Au(0) as the reaction intermediate. Furthermore, because Au_2O is thermodynamically unstable, it decomposes to metallic Au very quickly, especially at higher temperatures.

The ability to determine the dynamic electronic structure of the chemical site under working conditions with appropriate time resolution enables the determination of short-lived structures that are often responsible for the chemical reactivity. Flavell[36] said recently, "At present, the mechanisms of very few reactions are understood in detail — measurement techniques are usually too slow to monitor the intermediates formed. It is a bit like only being able to see who crosses the finishing line first in a race, and not how they got there." The proposed approach of using time-resolved RIXS enables us to follow the race and to determine all involved species. This is particularly important for gold chemistry, where there is large controversy with respect to the active oxidation state of gold. Most of the suggested active gold states were formulated based on pre- and postreaction analysis.

■ ASSOCIATED CONTENT

Supporting Information

The Experimental details, including theoretical calculations and genetic algorithm overview. This material is available free of charge via the Internet at http://pubs.acs.org.

■ AUTHOR INFORMATION

Corresponding Authors

*E-mail: jakub.szlachetko@psi.ch (J. Szlachetko).

*E-mail: stampfl@physics.usyd.edu.au (C. Stampfl).

Author Contributions

[∇]J. Szlachetko and J. Sá contributed equally to the manuscript.

Notes

The authors declare no competing financial interest.

■ ACKNOWLEDGMENTS

The authors would like to acknowledge the Swiss Light Source, from the Paul Scherrer Institute (Switzerland), for access to the X10DA (SuperXAS) beam line. The authors thank Prof. van Bokhoven for the fruitful discussions.

■ REFERENCES

(1) Hammer, B.; Nørskov, J. K. Why Gold is the Noblest of All the Metals. *Nature* **1995**, *376*, 238−240.
(2) Blingaard, T.; Nørskov, J. K.; Dahl, S.; Matthiesen, J.; Christensen, C. H.; Shested, J. The Brønsted−Evans−Polanyi Relation and the Volcano Curve in Heterogeneous Catalysis. *J. Catal.* **2004**, *224*, 206−217.
(3) Glatzel, P.; Singh, J.; Kvashnina, K. O.; van Bokhoven, J. A. In Situ Characterization of the 5d Density of States of Pt Nanoparticles upon Adsorption of CO. *J. Am. Chem. Soc.* **2010**, *132*, 2555−2557.
(4) Bauer, M.; Gastl, C. X-ray Absorption in Homogeneous Catalysis Research: The Iron-Catalyzed Michael Addition Reaction by XAS, RIXS and Multi-Dimensional Spectroscopy. *Phys. Chem. Chem. Phys.* **2010**, *12*, 5575−5584.
(5) Suljoti, E.; Garcia-Diez, R.; Bokarev, S. I.; Lange, K. M.; Schoch, R.; Dierker, B.; Dantz, M.; Yamamoto, K.; Engel, N.; Atak, K.; et al. Direct Observation of Molecular Orbital Mixing in a Solvated Organometallic Complex. *Angew. Chem., Int. Ed.* **2013**, *52*, 9841−9844.
(6) Dierker, B.; Suljoti, E.; Atak, K.; Lange, K. M.; Engel, N.; Golnak, R.; Dantz, M.; Hodeck, K.; Khan, M.; Kosugi, N.; Aziz, E. F. Probing Orbital Symmetry in Solution: Polarization-Dependent Resonant Inelastic Soft X-ray Scattering on Liquid Micro-Jet. *New J. Phys.* **2013**, *15*, 093025.
(7) Lange, K. M.; Aziz, E. F. Electronic Structure of Ions and Molecules in Solution: A View from Modern Soft X-ray Spectroscopies. *Chem. Soc. Rev.* **2013**, *42*, 6840−6859.
(8) See the issue on Progress in Resonant Inelastic X-ray Scattering: *J. Electron Spectrosc. Relat. Phenom.* **2013**, *188*, 1−182.
(9) Huotari, S.; Albergamo, F.; Vankó, G.; Verbeni, R.; Monaco, G. Resonant Inelastic Hard X-ray Scattering with Diced Analyzer Crystals and Position-Sensitive Detectors. *Rev. Sci. Instrum.* **2006**, *77*, 053102.
(10) Kleymenov, E.; van Bokhoven, J. A.; David, C.; Glatzel, P.; Janousch, M.; Alonso-Mori, R.; Studer, M.; Willimann, M.; Bergamaschi, A.; Henrich, B.; Nachtegaal, M. Five-Element Johann-Type X-ray Emission Spectrometer with a Single-Photon-Counting Pixel Detector. *Rev. Sci. Instrum.* **2011**, *82*, 065107.
(11) Kavčič, M.; Budnar, M.; Mühleisen, A.; Gasser, F.; Žitnik, M.; Bučar, K.; Bohinc, R. Design and Performance of a Versatile Curved-Crystal Spectrometer for High-Resolution Spectroscopy in the Tender X-ray Range. *Rev. Sci. Instrum.* **2012**, *83*, 033113.
(12) Szlachetko, J.; Nachtegaal, M.; de Boni, E.; Willimann, M.; Safonova, O.; Sá, J.; Smolentsev, G.; Szlachetko, M.; van Bokhoven, J. A.; Dousse, J.-Cl.; et al. A von Hamos X-ray Spectrometer Based on a Segmented-Type Diffraction Crystal for Single-Shot X-ray Emission Spectroscopy and Time-Resolved Resonant Inelastic X-ray Scattering Studies. *Rev. Sci. Instrum.* **2012**, *83*, 103105.
(13) Szlachetko, J.; Sá, J.; Safonova, O. V.; Smolentsev, G.; Szlachetko, M.; van Bokhoven, J. A.; Nachtegaal, M. In Situ Hard X-ray Quick RIXS to Probe Dynamic Changes in the Electronic Structure of Functional Materials. J. *Electron Spectrosc. Relat. Phenom.* **2013**, *188*, 161−165.
(14) Campbell, J. L.; Papp, T. Widths of the Atomic K−N7 Levels. *At. Data Nucl. Data Tables* **2001**, *77*, 1−56.
(15) Venugopal, A.; Aluha, J.; Scurrell, M. S. The Water−Gas Shift Reaction over Au-Based, Bimetallic Catalysts. The Au−M (M=Ag, Bi, Co, Cu, Mn, Ni, Pb, Ru, Sn, Tl) on Iron(III) Oxide System. *Catal. Lett.* **2003**, *90*, 1−6.
(16) Hereijgers, B. P. C.; Eggenhuisen, T. M.; de Jong, K. P.; Talsma, H.; van der Eerden, Ad M. J.; Beale, A. M.; Weckhuysen, B. M. Understanding the Promotion Effect of Lanthanum Oxide on Gold-Based Catalysts in the Partial Oxidation of Methanol by In Situ XAFS and DSC Studies. *J. Phys. Chem. C* **2011**, *115*, 15545−15554.
(17) Zhang, P.; Sham, T. K. X-ray Studies of the Structure and Electronic Behavior of Alkanethiolate-Capped Gold Nanoparticles: The Interplay of Size and Surface Effects. *Phys. Rev. Lett.* **2003**, *90*, 245502.
(18) Cho, D.-Y.; Park, J.; Yu, J.; Park, J.-G. X-ray Absorption Spectroscopy Studies of Spin−Orbit Coupling in 5d Transition Metal Oxides. *J. Phys.: Condens. Matter.* **2012**, *24*, 055503.
(19) Luke, B. T. Genetic Algorithms and Beyond. *Data Handl. Sci. Technol.* **2003**, *23*, 3−54.
(20) Yang, W. Y.; Cao, W.; Chung, T.-S.; Morris, J. *Optimization, in Applied Numerical Methods Using MATLAB®*; John Wiley & Sons, Inc.: Hoboken, NJ, 2005.
(21) Shi, H.; Asahi, R.; Stampfl, C. Properties of the Gold Oxides Au_2O_3 and Au_2O: First-Principles Investigation. *Phys. Rev. B* **2007**, *75*, 205125.
(22) Rehr, J. J.; Kas, J. J.; Prange, M. P.; Sorini, A. P.; Takimoto, Y.; Vila, F. D. Ab Initio Theory and Calculations of X-ray Spectra. *C. R. Phys.* **1999**, *10*, 548−559.
(23) Rehr, J. J.; Kas, J. J.; Vila, F. D.; Prange, M. P.; Jorissen, K. Parameter-Free Calculations of X-ray Spectra with FEFF9. *Phys. Chem. Chem. Phys.* **2010**, *12*, 5503−5513.
(24) Tulkki, J.; Aberg, T. Behaviour of Raman Resonance Scattering Across the K X-ray Absorption Edge. *J. Phys. B: At. Mol. Phys.* **1982**, *15*, L435.
(25) Christensen, N. E. Photoemission from Au{111} and {110}. Temperature Effects. *Phys. Rev. B* **1979**, *20*, 3205.
(26) Christensen, N. E.; Seraphin, B. O. Relativistic Band Calculation and the Optical Properties of Gold. *Phys. Rev. B* **1971**, *4*, 3321.
(27) Paniago, R.; Matzdorf, R.; Meister, G.; Goldmann, A. Temperature Dependence of Shockley-Type Surface Energy Bands on Cu(111), Ag(111) and Au(111). *Surf. Sci.* **1995**, *336*, 113−122.
(28) Kresse, G.; Hafner, J. Ab Initio Molecular Dynamics for Liquid Metals. *Phys. Rev. B* **1993**, *47*, 558.
(29) Kresse, G.; Hafner, J. Ab Initio Molecular-Dynamics Simulation of the Liquid-Metal−Amorphous-Semiconductor Transition in Germanium. *Phys. Rev. B* **1994**, *49*, 14251.
(30) Kresse, G.; Furthmüller, J. Efficiency of Ab-Initio Total Energy Calculations for Metals and Semiconductors Using a Plane-Wave Basis Set. *Comput. Mater. Sci.* **1996**, *6*, 15−50.
(31) Kresse, G.; Furthmüller, J. Efficient Iterative Schemes for Ab Initio Total-Energy Calculations Using a Plane-Wave Basis Set. *Phys. Rev. B* **1996**, *54*, 11169.
(32) Reuter, K.; Scheffler, M. Composition, Structure, and Stability of $RuO_2(110)$ as a Function of Oxygen Pressure. *Phys. Rev. B* **2001**, *65*, 035406.
(33) Kresse, G.; Joubert, D. From Ultrasoft Pseudopotentials to the Projector Augmented-Wave Method. *Phys. Rev. B* **1999**, *59*, 1758.
(34) Blöchl, P. E. Projector Augmented-Wave Method. *Phys. Rev. B* **1994**, *50*, 17953.
(35) Perdew, J. P.; Chevary, J. A.; Vosko, S. H.; Jackson, K. A.; Pederson, M. R.; Singh, D. J.; Fiolhais, C. Atoms, Molecules, Solids, and Surfaces: Applications of the Generalized Gradient Approximation for Exchange and Correlation. *Phys. Rev. B* **1992**, *46*, 6671.
(36) Flavell, W. R. Next Generation Advanced Light Source Science; *Proceedings of PAC07 IEEE*; 22nd PAC Conference, Albuquerque, NM, June 25−29, 2007.